Soil Biology and Biochemistry 133 (2019) 188–195

Contents lists available at ScienceDirect

Soil Biology and Biochemistry

journal homepage: www.elsevier.com/locate/soilbio

Impact of ecohydrological fluctuations on iron-redox cycling

Salvatore Calabrese[a,b,*], Amilcare Porporato[a,b]

[a] Department of Civil and Environmental Engineering, Princeton University, Princeton, NJ, USA
[b] Princeton Environmental Institute, Princeton University, Princeton, NJ, USA

ARTICLE INFO

Keywords:
Soil iron redox
Iron and carbon model
Hydrologic control
Soil moisture variability
Plant uptake

ABSTRACT

Because of its interaction with plants, carbon decomposition, and soil properties, soil iron cycle has been recognized as an important player in the carbon and other biogeochemical cycles. The impact of the hydrologic cycle and plants on it, however, remains largely unexplored. Here we focus on terrestrial ecosystems and develop a dynamical system to analyze the coupling between iron and carbon dynamics in the soil root zone as driven by fluctuations in soil moisture. Particular emphasis is placed on the modeling of the soil organic matter, the Fe-reducing population, the iron Fe^{2+}-Fe^{3+} cycling, and the soil moisture level, which controls the redox rates. Informed by laboratory and field measurements from a tropical forest, our results suggest that soil moisture and litterfall rates are the primary drivers of iron fluctuations at daily-to-seasonal temporal scales. We also emphasize the important role of soil iron cycle in the decomposition of the organic matter.

1. Introduction

The cyclic switching of soil iron between its reduced and oxidized states affects minerals cristallinity and sorbing properties (Thompson et al., 2006; Jones et al., 2009), and in turn controls the fate of dissolved species such as nutrients and organic matter (Zhao et al., 2016). This 'cycle' of iron also determines the availability of iron to plants as a micronutrient necessary to their growth (Frenzel et al., 1999; Colombo et al., 2014) (see for instance the fertilization experiment in the southern ocean (Coale et al., 1996; Blain et al., 2007)) and the biologically mediated iron reduction is fundamental to the decomposition of organic matter in environments experiencing anoxic conditions (Lovley and Phillips, 1986; Pasakarnis et al., 2015), such as humid tropical ecosystems (Dubinsky et al., 2010). For these reasons, soil iron dynamics plays a central role in the global carbon cycle.

Iron is often present in low soluble forms, posing stress on crops and limiting their yield (Guerinot and Yi, 1994). In the soil solution, Fe^{3+} derives mainly from dissimilatory Fe-reduction, a metabolism in which in anoxic conditions microbes rely on Fe^{3+} as an electron acceptor for organic matter mineralization (e.g., Lovley (1991); Colombo et al. (2014); Weber et al. (2006)). The soil redox state is affected by hydrologic fluctuations as soil moisture directly controls microbial respiration and the alternation of oxic/anoxic conditions (Rodríguez-Iturbe and Porporato, 2004; Todd-Brown et al., 2012). By consuming oxygen and producing carbon dioxide during organic carbon decomposition, microbial activity in fact affects the composition of the soil pore atmosphere (Daly et al., 2008; Brady and Weil, 2016), with a feedback on the redox conditions (Brady and Weil, 2016).

A few studies have explored mechanisms and rates of microbial Fe^{3+} reduction and its role in anaerobic environments (e.g., Lovley et al. (1991); Canfield et al. (1993); Kostka et al. (2002); Ginn et al. (2017); Barcellos et al. (2018a)), but have focused mainly on the biochemical aspects of the redox reaction in a laboratory setting. It was only recently that frequent ($\approx$ days) measurements of soil iron have started to be collected (Barcellos et al., 2018b), with the goal of exploring the environmental controls on Fe-reduction. Because of the complex interaction between ecohydrological and biochemical processes, only a joint analysis of soil iron and carbon cycles and soil water balance may provide the needed insights into soil iron dynamics to understand its role on carbon decomposition in various anoxic environments, such as wetlands and humid tropical forests (Liptzin et al., 2011). To the best of our knowledge no study has consistently linked all these aspects.

Existing geochemical transport models (e.g., Yeh and Tripathi (1991); Suarez and Simunek (1997); Saaltink et al. (2004)) aim at providing a detailed description of water flow and chemical reactions in space and time, but require numerical solution of partial differential equations with a large number of variables. This tends to hide the interaction between the various processes and makes these models unsuitable for a theoretical study of the coupling between iron and carbon cycles.

In this paper, we develop an analytical model that couples iron and

* Corresponding author. Department of Civil and Environmental Engineering, Princeton University, Princeton, NJ, USA.
E-mail address: sc58@princeton.edu (S. Calabrese).

https://doi.org/10.1016/j.soilbio.2019.03.013
Received 26 May 2018; Received in revised form 7 February 2019; Accepted 10 March 2019
Available online 13 March 2019
0038-0717/

carbon cycles in the soil root zone and that takes into account the soil moisture control on iron and carbon fluxes. The model is spatially lumped and consists of ordinary differential equations describing the time evolution of iron, Fe^{2+} and Fe^{3+}, carbon substrate and population of Fe-reducers. We model the redox reaction and the carbon decomposition by means of specific rate laws and introduce functions that account for the level of soil moisture. This spatially integrated formulation allows us to readily couple a model for soil moisture dynamics, whereby accounting for its impact on the redox fluctuations within the rhizosphere. As a case study, we analyze the soil iron cycle in the hot humid forest in the Luquillo Experimental Forest in Puerto Rico (LEF), which because of its climatic and soil features is characterized by very dynamic biogeochemical cycling and represents an optimal site for studying iron fluctuations.

2. Methods

We begin by presenting the details of the model and by describing the balance equations for iron, carbon and soil moisture. We then proceed with explaining the parameterization based on laboratory and field measurements on soils from the LEF.

2.1. Fe-C model

We use different compartments to model the time evolution of the state variables in a spatially lumped formulation representing vertical averages over the root zone (Fig. 1). The iron oxidation states are modeled using two separate compartments for the reduced state, Fe^{2+}, and the oxidized state, Fe^{3+}. With regard to the soil carbon, we adopt two different compartments to model the time evolution of the carbon substrate and the population of Fe-reducing microbes.

2.1.1. Fe-redox dynamics

At typical soil pHs, iron is present in the reduced state as Fe^{2+} and in the oxidized state as Fe^{3+} (Brady and Weil, 2016). Ferrous iron, Fe^{2+}, is originally found in primary minerals and is released into the soil solution as a product of mineral weathering, usually mediated by microorganisms (Weber et al., 2006; Colombo et al., 2014). Once dissolved in soil water, iron becomes available to plants and microbes to support their physiological processes and their growth, respectively. At high soil moisture levels (above the soil field capacity), however, iron is also lost by percolation to deeper soil layers and eventually to streams.

Within the root zone, fluctuations in soil moisture induce changes in soil air composition (oxic/anoxic conditions), thereby generating a continuous alternation of oxidizing and reducing conditions (Brady and Weil, 2016). On the one hand, in the presence of oxygen accepting electrons ferrous iron (Fe^{2+}) is readily oxidized to ferric iron (Fe^{3+}), which precipitates forming mostly short-range ordered Fe minerals (e.g., ferrihydrite), but also more crystalline phases (such as hematite)

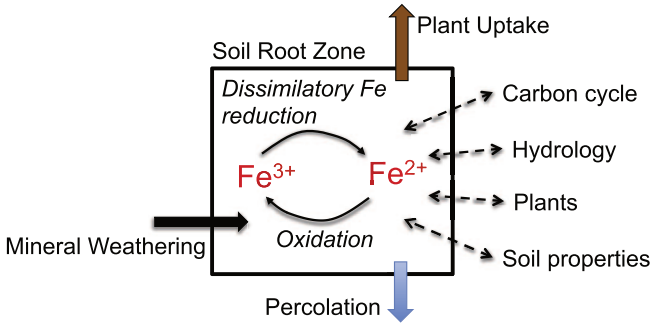

Fig. 1. Schematic representation of the iron-redox cycle in the soil root zone and its interactions with plants, hydrology, soil properties as well as carbon cycle. The Figure emphasizes the importance of all these aspects for understanding soil iron fluctuations. See description in section 2.1.

(Weiss et al., 2004, 2005; Thompson et al., 2006). Part of the oxidation occurs biologically (Fe-oxidizing bacteria) at rates that can be comparable to abiotic oxidation (Weber et al., 2006).

On the other hand, when oxygen is depleted Fe^{3+}-reducing microorganisms rely on the availability of Fe^{3+} as an electron acceptor and reduce it back to ferrous iron (Fe^{2+}) in order to decompose the organic matter (Lovley, 1991; Roden and Wetzel, 1996; Dubinsky et al., 2010).

The balance equations for iron in the two redox states can thus be expressed as

$$\frac{dFe^{2+}}{dt} = MW + RED - OX - UP - L_{Fe^{2+}}, \tag{1}$$

$$\frac{dFe^{3+}}{dt} = OX - RED, \tag{2}$$

where Fe^{2+} is the amount of dissolved ferrous iron and Fe^{3+} is the available short-ranged Fe^{3+} phases. The terms OX and RED are the oxidation and reduction rates, respectively, MW (mineral weathering) is the release of iron Fe^{2+} from highly crystalline Fe minerals, UP is the iron uptake by plants, and $L_{Fe^{2+}}$ is the loss of iron as leaching.

Mineral weathering, MW, represents the slow release of iron from Fe-minerals, which provide a source of iron over long timescales. Since it is small and varies slowly compared to the fast dynamics of Fe^{2+}-Fe^{3+} cycling, this term can be considered as constant.

The reduction and oxidation processes are modeled by means of semi-empirical kinetic laws. The reduction rate of Fe^{3+}, associated to the decomposition of the organic matter, C, is modeled through a multiplicative function of the population of Fe-reducers, BM, the carbon substrate, C, and the availability of short-ranged Fe^{3+} minerals,

$$RED = f(s)k_{red}\cdot BM\cdot C\cdot Fe^{3+}, \tag{3}$$

while the oxidation rate is modeled as (Stumm and Morgan, 2012; Ginn et al., 2017)

$$OX = g(s)k_{ox}(Fe^{2+} - Fe_0^{2+}), \tag{4}$$

where Fe_0^{2+} is a small fraction of the iron pool that is resistant to oxidation, likely due to physical protection (Ginn et al., 2017). In agreement with observations (Brady and Weil, 2016), the factor $f(s)$ limits the reduction rate at low soil moisture levels, at which aeration suppresses anaerobic processes. Below field capacity, high oxygen levels inhibit anaerobic processes, and $f = 0$, while as soil moisture increases, f nonlinearly increases and reaches 1 at saturation,

$$f(s) = \begin{cases} 0 & s < s_{fc}, \\ \left(\frac{s - s_{fc}}{1 - s_{fc}}\right)^{\beta} & s > s_{fc}, \end{cases} \tag{5}$$

where we set $\beta = 2$.

On the other hand, field measurements show that soil moisture is essentially a proxy for oxygen content (Hall et al., 2013). Oxygen levels remain very high (close to the atmospheric value) up to soil moisture at field capacity and then quickly decline nonlinearly (Fig. 2(a)) as the soil approaches saturation. Accordingly, to account for oxygen limitation at high soil moisture levels, the function $g(s)$ is modeled as

$$g(s) = \begin{cases} 1 & s < s_{sfc}, \\ 1 - \left(\frac{s - s_{fc}}{1 - s_{fc}}\right)^{\zeta} & s > s_{fc}. \end{cases} \tag{6}$$

Iron uptake, UP, occurs through the roots as the plant takes in water for transpiration. It is a function of soil moisture and concentration of Fe^{2+} and can be computed as

$$UP = T(s)[Fe^{2+}] = T(s)\frac{Fe^{2+}}{nsZ_r}, \tag{7}$$

in which Z_r is the depth of root zone. The transpiration rate, $T(s)$, is modeled as an increasing function of soil moisture accounting for the plant stomatal response to water stress (Porporato et al., 2003) and its

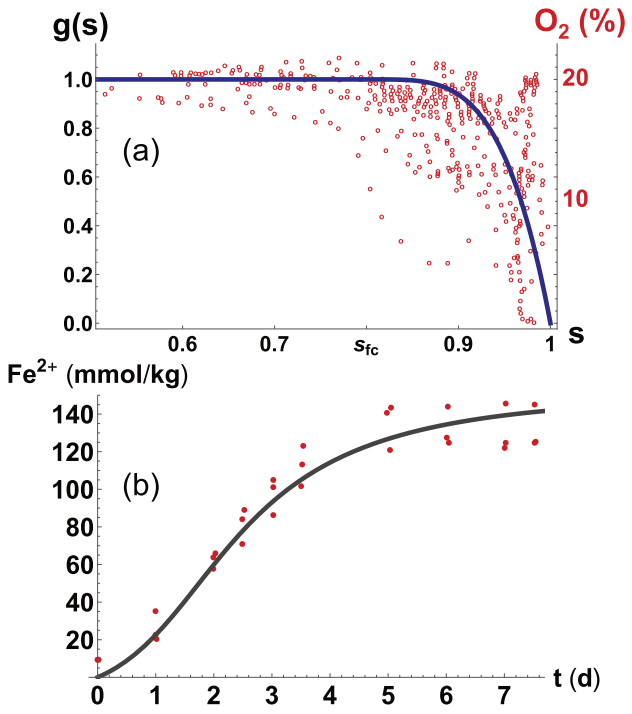

Fig. 2. Panel (a): The solid line illustrates the control factor $g(s)$ accounting for oxygen limitation at high soil moisture levels, while the red circles are oxygen and soil moisture measurements from the Luquillo Experimental Forest (LEF) by Hall et al. (2013). For this study, $\zeta = 4$. Panel (b): Calibration of the reduction rate constant. The red point are the results of the reduction experiment by Ginn et al. (2017), in which soil samples were kept for 7 days in anoxic conditions without substrate and Fe-reducers limitations. The solid line refers to the modeled evolution of Fe^{2+} after calibration. To simulate the anoxic conditions, the model was run for constant soil moisture $s = 1$ (saturation), whereas to avoid substrate and Fe-reducers limitation, the initial condition was set to $Fe^{2+} = 0$ mmol/kg, $C = 20$ g/kg, and $BM = 5{\cdot}10^{11}$ cells/kg. (For interpretation of the references to colour in this figure legend, the reader is referred to the Web version of this article.)

specific formula is shown in section 2.1.3 below.

Finally, the loss of Fe^{2+} via percolation can be similarly computed as

$$L_{Fe^{2+}} = L(s)[Fe^{2+}] = L(s)\frac{Fe^{2+}}{nsZ_r}, \tag{8}$$

where the percolation rate $L(s)$, which is zero below field capacity, is a function of soil moisture, hydraulic conductivity, and soil type (Rodríguez-Iturbe and Porporato, 2004), see section 2.1.3.

2.1.2. C dynamics

We model the time evolution of the soil organic carbon and the population of Fe-reducers through the following balance equations,

$$\frac{dC}{dt} = ADD + BD - DEC_{aer} - DEC_{red}, \tag{9}$$

and

$$\frac{dBM}{dt} = G_{BM} - BD. \tag{10}$$

The term ADD represents the deposition of plant residues, such as leaves, roots and branches, which become available to microbial colonies for their metabolism, whereas BD, biomass decay, is the carbon recycled through death of the microbial biomass, generally assumed to be a linear decay, i.e., $BD = k_{bd}BM$ (Porporato et al., 2003; Manzoni and Porporato, 2007).

The output is given by the decomposition through aerobic metabolism, DEC_{aer}, and dissimilatory iron reduction, DEC_{red}. The decomposition of the substrate by the aerobic biomass is modeled by means of first order kinetics,

$$DEC_{aer} = k_{aer}\phi(s)C, \tag{11}$$

where k_{aer} is the aerobic decomposition rate. The function $\phi(s)$ accounts for water limitation at low soil moisture and oxygen limitation at high soil moisture, and is modeled as an increasing linear function up to soil field capacity, $s = s_{fc}$, and an hyperbolic decay for soil moisture levels above field capacity (Cabon et al., 1991; Brady and Weil, 2016).

Because the decomposition through iron reduction is proportional to the moles of iron reduced, it follows that $DEC_{red} = \beta RED$, where β represents the grams of carbon decomposed per mole of iron reduced. This constant is computed considering that chemical analyses show an average C content in the organic matter of 45% and that 4 mol of carbon are decomposed per mol of iron reduced (Lovley and Phillips, 1986; Kostka et al., 2002; Hall et al., 2013). Finally, the growth of Fe-reducers has been shown to be proportional to the moles of iron reduced (Kostka et al., 2002), so that $G = rRED$.

2.1.3. Soil moisture dynamics

The balance equation for the root zone soil moisture is written as Laio et al. (2001),

$$nZ_r\frac{ds}{dt} = R - Q - E - T - L, \tag{12}$$

where n is the soil porosity, Z_r is the depth of the root zone, and s is the soil moisture expressed in terms of saturation. The product $nZ_r s$ thus represents the total volume of water per unit ground area. The term R is the rainfall rate, Q is the runoff generated when rainfall exceeds the soil storage capacity ($nZ_r(1 - s)$), whereas E, T and L are the water losses as evaporation, transpiration and percolation, respectively.

Available rainfall data at daily timescale cover only a period of approximately 25 years with occasional gaps. To overcome such a limitation and account for the long term effect of the intermittent and random nature of rainfall, we also model R as a marked Poisson process with event frequency λ, representing the inverse of the mean inter-arrival times between two subsequent rainfall events, and random rainfall depths that are exponentially distributed with mean depth α (Rodríguez-Iturbe and Porporato, 2004). Frequency and mean rainfall depth are derived from the rainfall dataset as shown in section 2.2.3 below (Fig. 3).

For simplicity, the evaporation E is modeled as a linear, increasing function of soil moisture from $E = 0$ at the hygroscopic point, s_h, to E_{max} at the soil wilting point, s_w, E_{max} being the potential evaporation. To account for plant stomatal response to water stress, we model also transpiration as an increasing function of soil moisture from 0 at $s = s_w$ to T_{max} at the soil moisture level at which plants begin to suffer from water stress, which we refer to as s^*.

When the soil moisture exceeds the soil field capacity, s_{fc}, water is lost also by percolation due to gravity, L. We compute this loss as a power law function of soil moisture, $L = k_h s^c$, where k_h is the hydraulic conductivity and c is an empirical parameter depending on soil texture (Clapp and Hornberger, 1978; Laio et al., 2001).

2.2. Case study

Our study area is the subtropical humid forest in the Bisley watershed of the Luquillo Experimental Forest in Puerto Rico (Scatena, 1989). The site is characterized by a low seasonal climate with about 3500 mm/year of average precipitation. Based on the USDA classification, these soils are mostly classified as Ultisols that formed from volcanic parent material. Top soils (40 cm) in upland locations can be considered silty clay loams according to the USDA texture classification, with an average porosity of 0.48 and bulk density of 0.7 g/cm^3 (Hall et al., 2013), but there are large textural variations across

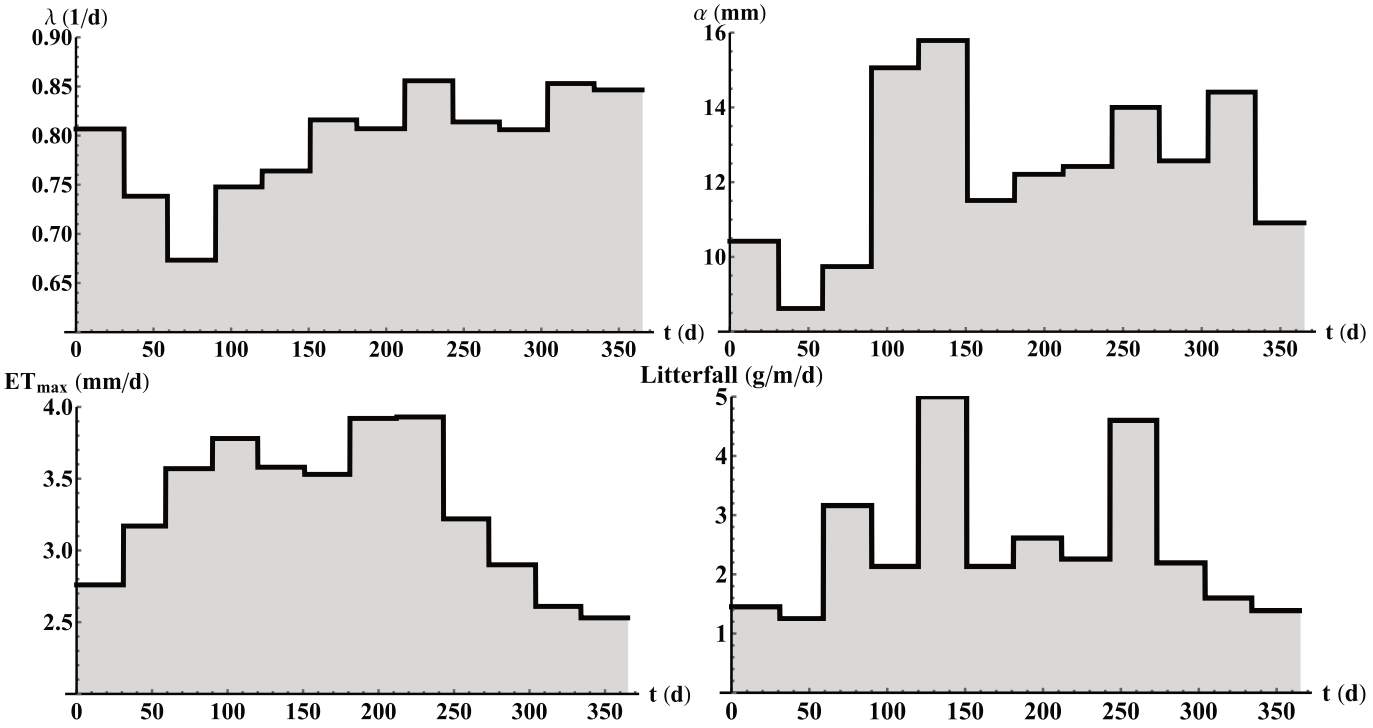

Fig. 3. Monthly evolution of the climatic parameters and the litterfall rates at the Bisley watershed (LEF, Puerto Rico).

elevation gradients. The Luquillo Experimental Forest (LEF) is a Long Term Ecological Research site (https://luq.lter.network/) and a Critical Zone Observatory (https://criticalzone.org/luquillo/), through which biogeochemical observations are available since 1988.

2.2.1. Parameterization of Re-redox rates

The total iron content in these soils is about 1150 mmol/kg soil, of which 150 mmol/kg is in short-range ordered or low-crystallinity Fe^{3+} phases (Ginn et al., 2017; Barcellos et al., 2018a). The remaining portion is in more crystalline phases (e.g., goethite) or is dissolved in water in the reduced state (Fe^{2+}).

The reduction rate constant, k_{red}, was calibrated with the reduction experiments by Ginn et al. (2017), in which soil samples were placed for 7 days in anoxic conditions, after being exposed for 28 days to an alternation of oxic and anoxic conditions. We solved the model to fit the experimental data, considering constant anoxic conditions ($s = 1$), high substrate and Fe-reducers contents, and an initial condition $Fe^{2+} = 0$ (see Fig. 2(b)). The oxidation rate constant, k_{ox}, for the oxidation rate law (4) was calibrated by Ginn et al. (2017) to model the decrease in Fe^{2+} concentrations during oxic conditions observed in their experiments.

2.2.2. Parameterization of microbial growth and C decay

We parameterize the growth of Fe-reducers based on growth yields experiments by Kostka et al. (2002), which showed that microbial growth was proportional to the reduction rate and the coefficient of proportionality (expressing the growth per mole of Fe^{3+} reduced) was about $5{\cdot}10^{10}$ cells/moles. The microbial decay rate was determined by fitting an exponential decay to the decrease of Fe-reducers observed in soil samples kept in oxic conditions in the experiments by Ginn et al. (2017).

The input of carbon, ADD, was determined according to measurements of litterfall rate (Zou et al., 1995). In particular, we imposed for each day a litterfall rate equal to the average rate for the specific month. The decay rate, k_{aer}, due to aerobic substrate decomposition was selected in accordance with results from litterbag experiments (Bloomfield et al., 1993).

2.2.3. Parameterization of climatological and soil parameters

We gathered longterm rainfall data, from 1988 to 2015, from the LTER website (https://luq.lter.network/data/luqmetadata148/7469). To take into account the seasonality in precipitation, we computed the rainfall frequency, λ, and mean rainfall depth, α, separately per each month. The results, shown in Fig. 3(a) and (b), are consistent with previous estimates of rainfall statistics (Heartsill-Scalley et al., 2007).

The potential evapotranspiration, ET_{max}, was acquired from the CRU climate dataset (Harris et al., 2014), which provides monthly values for land surface climatological variables. Similarly to rainfall, we computed long term averages of potential evapotranspiration per each month (Fig. 3(c)). We then assumed that the potential evaporation (E_{max}) has a constant value of 1 mm/day, so that per each month $T_{max} = ET_{max} - E_{max}$.

Soil porosity and hydraulic conductivity were selected according to typical values for silty clay loams (Clapp and Hornberger, 1978; Fernandez-Illescas et al., 2001), while soil moisture at the hygroscopic point, wilting point, incipient water stress were computed from the retention curve (Clapp and Hornberger, 1978; Laio et al., 2001) by assuming water potentials of -10, -3 and -0.03 MPa, respectively. Soil moisture at field capacity was set at 0.8, slightly above the value of s^*.

3. Results and discussion

Equations (1), (2), (9) and (10) form a dynamical system of ordinary differential equations for the four state variables: Fe^{2+}, Fe^{2+} concentration (mmol/kg^3 soil), Fe^{3+}, Fe^{3+} concentration (mmol/kg soil), C, carbon substrate concentration (g/kg soil), and BM, population of Fe-reducers (cells/kg soil). We integrated the equations numerically with a standard solver by setting an initial condition close to typical values observed in field measurements. We then let the model run for a period of time long enough (100 years) that the influence of the initial condition became negligible. The results, discussed below, are shown in time Fig. 4.

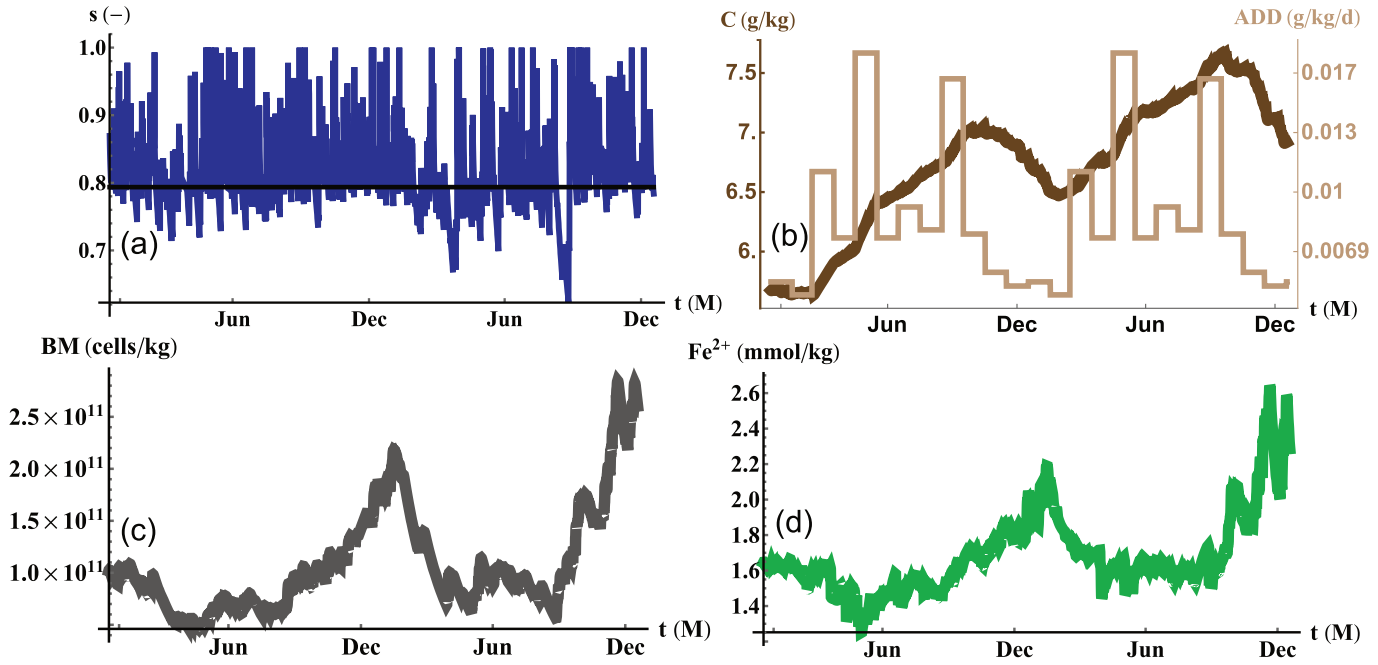

Fig. 4. Temporal evolution of soil moisture (a), carbon substrate and litterfall rates (b), population of Fe-reducers (c), and Fe^{2+} concentration (d) for a period of two years. The trajectories were computed by solving numerically equations (1), (2), (9) and (10). The Figure highlights the high frequency variability induced by soil moisture fluctuations and the seasonal variability caused by changes in litterfall rates. The values for the parameters can be found in Table 1.

Table 1
Ecohydrological and biochemical parameters at the Bisley watershed (LEF, Puerto Rico).

	Symbol	Value	Units[1]
Soil and vegetation parameters[a]			
Porosity	n	0.48	–
Depth of the root zone	Z_r	0.4	m
Soil hygroscopic point	s_h	0.36	–
Soil wilting point	s_w	0.42	–
Point of incipient water stress	s^*	0.76	–
Soil field capacity	s_{fc}	0.8	–
Biochemical and kinetic parameters			
Aerobic decomposition rate[b]	k_{aer}	$2.7\cdot10^{-4}$	1/d
Mole specific decomposition rate[c]	β	0.1	gC/mmol
Fe-reducers growth factor[d]	r	$5\cdot10^{10}$	cells/moles
Mineral weathering rate[e]	MW	0.08	mmol/kg/d
Reduction rate constant[f]	k_{red}	$8.89\cdot10^{-15}$	kg^2/cells/g/d
Oxidation rate constant[f]	k_{ox}	432	1/d

[a] From Hall et al. (2013).
[b] From Bloomfield et al. (1993).
[c] Computed considering that on average the soil organic matter here consists for the 45% of C (Bloomfield et al., 1993) and that 4 mol of C are oxidized per mol of Fe reduced (Kostka et al., 2002; Dubinsky et al., 2010).
[d] From Kostka et al. (2002).
[e] This study.
[f] Calibrated from Ginn et al. (2017), see Section 2.2.1.

3.1. Iron dynamics

The constant wet soil conditions, with soil moisture levels most of the time above field capacity ($s_{fc} = 0.8$), generate optimal conditions for anaerobic processes and Fe^{2+}-Fe^{3+} cycling. The frequent occurrence of anoxic conditions stimulates the use of Fe as electron acceptor for carbon decomposition, and hence the growth of the Fe-reducers and Fe reduction. The population of Fe-reducers remains large, of the order of 10^{11} cells/kg (Fig. 4(c)), throughout the entire simulated period, in agreement with field measurements that estimated a population up to 10^{12} cells/kg (Dubinsky et al., 2010). Throughout the simulated period, the soil carbon pool has on average approximately 7.5 g/kg of organic matter with a seasonality led by the variability in litterfall rates (Fig. 4(b)).

The dynamics of Fe^{2+} has high variability at various frequencies (Fig. 4(d)). Daily soil moisture fluctuations have immediate effects on the Fe-redox state, consistently with fast redox fluctuations observed in laboratory experiments (Ginn et al., 2017). In wet soil conditions ($s > s_{fc}$), Fe^{2+} values quickly grow above 2 mmol/kg and have peaks of 7–8 mmol/kg (see also Fig. 5), while exposures to high oxygen levels during dryer conditions ($s < s_{fc}$) rapidly deplete the Fe^{2+} pool. The time evolution of Fe^{2+} shows also a seasonal variability. Higher litterfall rates provide more carbon to Fe-reducers, which in turn grow and further stimulate net Fe reduction rates. As a result, higher values of both population of Fe-reducers and Fe^{2+} tend to occur during high litterfall deposition.

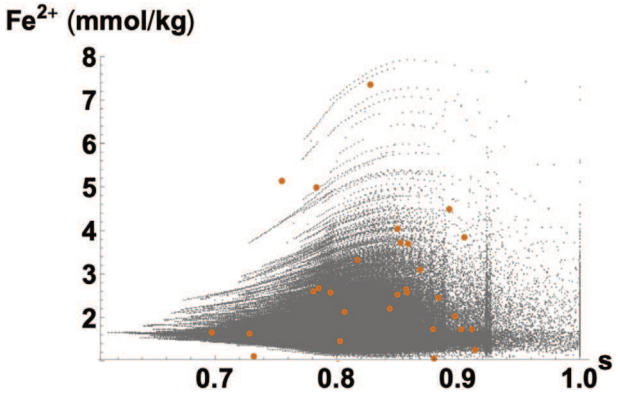

Fig. 5. Fe^{2+}-s phase space showing the region of Fe^{2+} and s values explored by the simulation and by field observations. The gray points were drawn from the simulation at a constant interval of 0.1 day, while the orange points are field measurements from the Espíritu Santu watershed (Barcellos et al., 2018b). The Figure reveals the region that is most explored by modeled and observed Fe^{2+} levels. (For interpretation of the references to colour in this figure legend, the reader is referred to the Web version of this article.)

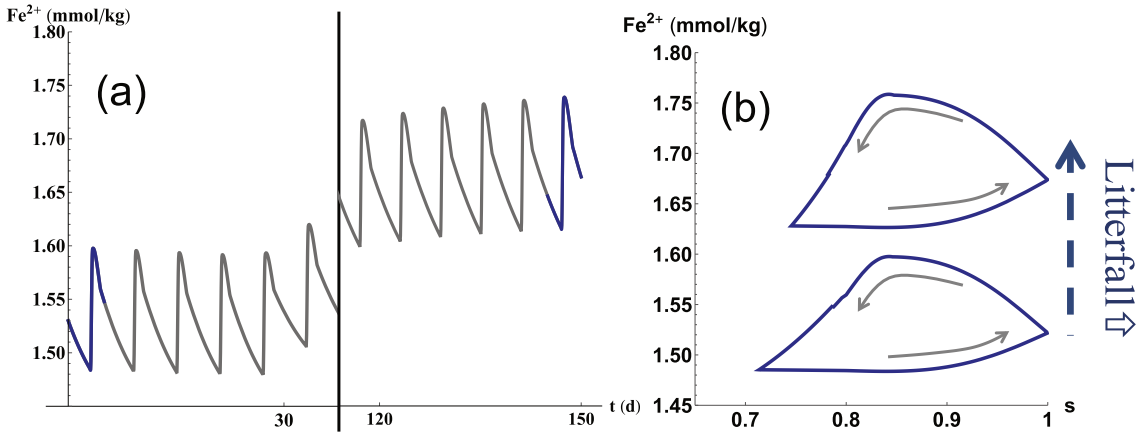

Fig. 6. Panel (a): Temporal evolution of Fe^{2+} showing the soil wetting and drying cycles as the litterfall rates increase. The trajectories were computed by solving equations (1), (2), (9) and (10) and the soil moisture dynamics (12) with deterministic rainfall, one event every six days that brings the soil to saturation. Panel (b): Time evolution of the system trajectory in the Fe^{2+}-*s* phase space. The trajectories form loops that are traveled in a counterclockwise direction during a wetting and drying cycle and explore higher Fe^{2+} values as litterfall rates increase.

3.2. Coupled Fe and soil moisture dynamics

The dependence of Fe^{2+} on soil moisture is illustrated in the Fe^{2+}-*s* phase space (Fig. 5), where the gray points were drawn from the simulated time evolution of Fe^{2+} and soil moisture at a constant time interval of 0.1 day. From the density of points in Fig. 5, it is evident that the region that is most explored is between soil moisture levels of 0.8 and 0.9. Due to the climate, lower soil moisture values are rare while higher levels approaching saturation are explored for short intervals, because water is quickly lost via percolation. Field measurements of soil moisture and Fe^{2+} from the Espíritu Santu watershed (Barcellos et al., 2018b), close to the Bisley watershed, fall within the cloud of gray points, and the highest values of Fe^{2+} are also observed at soil moisture just above field capacity. It is clear from Fig. 5, however, that more frequent measurements are needed for a thorough model-data comparison.

The response of the redox reaction to the soil moisture and litterfall dynamics is further explored in Fig. 6. During a soil wetting and drying cycle (Fig. 6(a)) the trajectories form loops in the Fe^{2+}-s phase space that are traveled in a counterclockwise direction (Fig. 6(b)). As we have seen above, when litterfall provides more carbon to the Fe-reducers, their population grow and more Fe is reduced. As a consequence, trajectories explore higher Fe^{2+} values for given soil moisture levels, forming loops in upper regions of the phase space. Interestingly, in the phase space given by the reduction rate and soil moisture (Fig. 7), the system trajectories collapse approximately on a single line, suggesting that the iron reduction rate can be uniquely related to the soil moisture level, while the effects of different litterfall rates and carbon contents appear negligible.

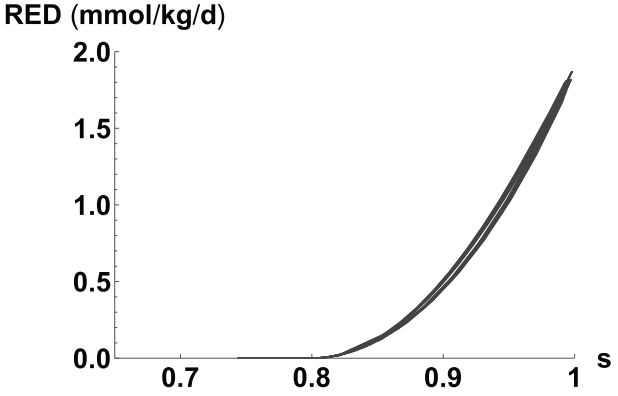

Fig. 7. Time evolution of the system trajectory in the *RED-s* phase space. From the trajectories computed in Fig. 6, we computed the reduction rate by means of equation (3).

3.3. Fe fluxes and carbon decomposition

From equations (3), (4), (7) and (8), we computed the temporal dynamics of the iron fluxes, namely reduction, oxidation, uptake and leaching. The long term average value for each flux is shown in Table 2. From the total overall input of iron ($MW = 0.08$ mmol/kg), approximately 0.06 mmol/kg leave the soil as leaching while the remaining 0.02 mmol/kg are taken up by plants. It is thus evident that an important role in Fe dynamics is played by plants, which account for 25% of soil iron losses. The average reduction rate is about 0.075 mmol/kg/d, with instantaneous rates approaching 10 mmol/kg/d, of the same order of values observed in laboratory experiments (2–50 mmol/kg/d) (Yang and Liptzin, 2015; Hall et al., 2016; Barcellos et al., 2018a).

Considering that four moles of carbon are decomposed per mole of Fe^{3+} reduced (Kostka et al., 2002; Dubinsky et al., 2010), iron reduction has the potential to drive the carbon cycle during periods of high soil moisture levels, in which the decomposition due to aerobic metabolism is inhibited (Brady and Weil, 2016). Because of soil moisture levels almost constantly above field capacity, our results in fact emphasize the importance of iron reduction as primary contributor to microbial respiration, in line with prior work estimating that in the wetter spots of these forests > 50% of the organic matter is decomposed through iron reduction (Dubinsky et al., 2010).

3.4. The effect of plant uptake on Fe redox

As we have shown above, soil iron dynamics is also impacted by the presence of plants, which uptake Fe^{2+} to sustain their physiological processes, such as photosynthesis, respiration, as well as the synthesis of chlorophyll (Kim and Guerinot, 2007). While iron deficiency results in chlorosis, namely the yellowing of the younger leaves, and growth-rate reduction (Mengel, 1994), high iron contents are toxic to plants due to the formation of hydroxyls radicals that damage the DNA,

Table 2
Longterm average of iron fluxes (mmol/kg/d) and of carbon decomposition rate (g/kg/d).

	MW	Reduction (Oxidation)	Uptake	Leaching	DEC_{red}
Value	0.08	0.075	0.02	0.06	0.0075

proteins and other cell components (Foy et al., 1978). Our results show that on average plant uptake contribute 25% to soil iron losses (Table 2) and is an important component of the soil iron cycle that cannot be neglected. The highest uptake rates are observed when soil moisture is at field capacity, as both transpiration rates and Fe^{2+} contents are high. At higher soil moisture, dilution prevails and the concentration of dissolved Fe^{2+} quickly decreases, whereas at low soil moisture plants reduce the uptake of iron because of water stress.

Because of the low concentrations of iron in the soil solution, the passive uptake of iron through transpiration may not be sufficient for plants to maintain optimal iron contents for their growth (Guerinot and Yi, 1994; Mori, 1999; Robinson et al., 1999). To overcome this limitation, plants have developed two possible strategies of active uptake. In strategy 1, typical of dicots and non-graminaceous monocots, roots enhance Fe^{3+} reduction by releasing protons and acidificating the rhizosphere and then transporting Fe through the root cell membranes. In strategy 2 (monocots), roots release ligands to form chelates with Fe^{3+} and then uptake it by means of a specific transporter. Through specific mechanisms, these plants can also uptake Fe-chelated forms deriving from microbial activity (Robin et al., 2008; Colombo et al., 2014). On the other hand, the mechanisms through which plants avoid toxic iron concentrations are not completely understood (Foy et al., 1978). It seems, however, that plants are able to induce oxidation of Fe^{2+} on the roots as well as to limit the internal translocation of iron (Bartlett, 1961).

These plant strategies become extremely important when interested in the effects of soil iron dynamics on crops. In this regard, models could account for plant strategies by introducing specific controlling factors in the oxidation and reduction rates, and an uptake term for Fe^{3+}, that depend on the plant-specific physiological demand of iron. This would make it possible to analyze also the feedback that different plant species and their active uptake have on soil iron and carbon cycles, fostering the design of novel detailed experiments to calibrate the controlling factors of the model component.

4. Conclusions

We have developed a dynamical system for the time evolution of iron and carbon concentrations and soil moisture in the soil root zone to explore the iron-carbon coupling and the control that the hydrologic regime exerts on them. The parsimony of this model allowed us to analyze the main relationships between the state variables and fluxes as well as to explore in detail the role of soil moisture dynamics. The model was used to analyze iron fluctuations at the Luquillo Experimental Forest, which due to its climate and soil characteristics represents an ideal location for studying the Fe cycle, and for which laboratory and field measurements were available.

Our results point to soil moisture and carbon as the main controllers of the soil iron cycle. Daily soil moisture variability induces changes in the concentration of oxygen and determine the transition between oxic and anoxic conditions. This in turn stimulates rapid Fe^{2+} fluctuations. Over monthly timescales, the concentration of the carbon substrate responds to the variability in litterfall rates, introducing a seasonal component into iron dynamics. Due to the complex dynamics coupling the soil moisture, carbon, and Fe^{2+}, the dependence of Fe^{2+} on soil moisture gives rise to hysteretic behaviors, see Fig. 6. On the contrary, the model reveals a simple increasing relationship between the reduction rate and the soil moisture level.

Soil conditions are mostly favorable to leaching of iron, which in the longterm accounts for $\approx$75% of total iron losses, but plants contribute substantially to the soil iron cycle by taking up the remaining 25%. During anoxic conditions, iron reduction approaches rates of 10 mmol/kg/d and is the main driver of microbial respiration.

Our analysis couples a variety of biotic and abiotic processes spanning a wide range of timescales, thus making it difficult to carry out detailed experiments to analyze their properties. In this regard, we hope that this model will be useful to design suitable experiments to capture these interactions as well as test hypotheses about their response to natural and human perturbations, such as hurricanes, drought, and agriculture. We also wish to bring to our attention the effect of different responses of plant types to iron deficiency and toxicity and their feedback on the soil iron dynamics. A model-experiment combination may provide detailed insights into this highly intertwined interaction between the hydrologic and the soil biogeochemical cycles.

Declaration of interests

None.

Acknowledgments

This work was supported through the USDA Agricultural Research Service cooperative agreement 58-6408-3-027; and National Science Foundation grants EAR-1331846, FESD-1338694, EAR-1316258. This work is a theoretical study and hence no data were produced. We thank Aaron Thompson and Diego Barcellos for the useful discussion. Valuable suggestions from the Associate Chief Editor Evgenia Blagodatskaya and the anonymous reviewers are gratefully acknowledged.

References

Barcellos, D., Cyle, K.T., Thompson, A., 2018a. Faster redox fluctuations can lead to higher iron reduction rates in humid forest soils. Biogeochemistry 137 (3), 367–378.
Barcellos, D., OConnell, C., Silver, W., Meile, C., Thompson, A., 2018b. Hot spots and hot moments of soil moisture explain fluctuations in iron and carbon cycling in a humid tropical forest soil. Soil Systems 2 (4), 59.
Bartlett, R., 1961. Iron oxidation proximate to plant roots. Soil Science 92 (6), 372–379.
Blain, S., Quéguiner, B., Armand, L., Belviso, S., Bombled, B., Bopp, L., Bowie, A., Brunet, C., Brussaard, C., Carlotti, F., et al., 2007. Effect of natural iron fertilization on carbon sequestration in the southern ocean. Nature 446 (7139), 1070.
Bloomfield, J., Vogt, K.A., Vogt, D.J., 1993. Decay rate and substrate quality of fine roots and foliage of two tropical tree species in the luquillo experimental forest, Puerto Rico. Plant and Soil 150 (2), 233–245.
Brady, N.C., Weil, R.R., 2016. The Nature and Properties of Soils. Pearson.
Cabon, F., Girard, G., Ledoux, E., 1991. Modelling of the nitrogen cycle in farm land areas. Fertilizer Research 27 (2–3), 161–169.
Canfield, D.E., Thamdrup, B., Hansen, J.W., 1993. The anaerobic degradation of organic matter in Danish coastal sediments: iron reduction, manganese reduction, and sulfate reduction. Geochimica et Cosmochimica Acta 57 (16), 3867–3883.
Clapp, R.B., Hornberger, G.M., 1978. Empirical equations for some soil hydraulic properties. Water Resources Research 14 (4), 601–604.
Coale, K.H., Johnson, K.S., Fitzwater, S.E., Gordon, R.M., Tanner, S., Chavez, F.P., Ferioli, L., Sakamoto, C., Rogers, P., Millero, F., et al., 1996. A massive phytoplankton bloom induced by an ecosystem-scale iron fertilization experiment in the equatorial pacific ocean. Nature 383 (6600), 495.
Colombo, C., Palumbo, G., He, J.-Z., Pinton, R., Cesco, S., 2014. Review on iron availability in soil: interaction of fe minerals, plants, and microbes. Journal of Soils and Sediments 14 (3), 538–548.
Daly, E., Oishi, A.C., Porporato, A., Katul, G.G., 2008. A stochastic model for daily subsurface co 2 concentration and related soil respiration. Advances in Water Resources 31 (7), 987–994.
Dubinsky, E.A., Silver, W.L., Firestone, M.K., 2010. Tropical forest soil microbial communities couple iron and carbon biogeochemistry. Ecology 91 (9), 2604–2612.
Fernandez-Illescas, C.P., Porporato, A., Laio, F., Rodriguez-Iturbe, I., 2001. The ecohydrological role of soil texture in a water-limited ecosystem. Water Resources Research 37 (12), 2863–2872.
Foy, C., Chaney, R. t., White, M., 1978. The physiology of metal toxicity in plants. Annual Review of Plant Physiology 29 (1), 511–566.
Frenzel, P., Bosse, U., Janssen, P.H., 1999. Rice roots and methanogenesis in a paddy soil: ferric iron as an alternative electron acceptor in the rooted soil. Soil Biology and Biochemistry 31 (3), 421–430.
Ginn, B., Meile, C., Wilmoth, J., Tang, Y., Thompson, A., 2017. Rapid iron reduction rates are stimulated by high-amplitude redox fluctuations in a tropical forest soil. Environmental Science and Technology 51 (6), 3250–3259.
Guerinot, M.L., Yi, Y., 1994. Iron: nutritious, noxious, and not readily available. Plant Physiology 104 (3), 815.
Hall, S.J., Liptzin, D., Buss, H.L., DeAngelis, K., Silver, W.L., 2016. Drivers and patterns of iron redox cycling from surface to bedrock in a deep tropical forest soil: a new conceptual model. Biogeochemistry 130 (1–2), 177–190.
Hall, S.J., McDowell, W.H., Silver, W.L., 2013. When wet gets wetter: decoupling of moisture, redox biogeochemistry, and greenhouse gas fluxes in a humid tropical forest soil. Ecosystems 16 (4), 576–589.
Harris, I., Jones, P.D., Osborn, T.J., Lister, D.H., 2014. Updated high-resolution grids of

monthly climatic observations–the cru ts3. 10 dataset. International Journal of Climatology 34 (3), 623–642.
Heartsill-Scalley, T., Scatena, F.N., Estrada, C., McDowell, W., Lugo, A.E., 2007. Disturbance and long-term patterns of rainfall and throughfall nutrient fluxes in a subtropical wet forest in Puerto Rico. Journal of Hydrology 333 (2–4), 472–485.
Jones, A.M., Collins, R.N., Rose, J., Waite, T.D., 2009. The effect of silica and natural organic matter on the fe (ii)-catalysed transformation and reactivity of fe (iii) minerals. Geochimica et Cosmochimica Acta 73 (15), 4409–4422.
Kim, S.A., Guerinot, M.L., 2007. Mining iron: iron uptake and transport in plants. FEBS Letters 581 (12), 2273–2280.
Kostka, J.E., Dalton, D.D., Skelton, H., Dollhopf, S., Stucki, J.W., 2002. Growth of iron (iii)-reducing bacteria on clay minerals as the sole electron acceptor and comparison of growth yields on a variety of oxidized iron forms. Applied and Environmental Microbiology 68 (12), 6256–6262.
Laio, F., Porporato, A., Ridolfi, L., Rodriguez-Iturbe, I., 2001. Plants in water-controlled ecosystems: active role in hydrologic processes and response to water stress: ii. probabilistic soil moisture dynamics. Advances in Water Resources 24 (7), 707–723.
Liptzin, D., Silver, W.L., Detto, M., 2011. Temporal dynamics in soil oxygen and greenhouse gases in two humid tropical forests. Ecosystems 14 (2), 171–182.
Lovley, D.R., 1991. Dissimilatory fe (iii) and mn (iv) reduction. Microbiological Reviews 55 (2), 259–287.
Lovley, D.R., Phillips, E.J., 1986. Organic matter mineralization with reduction of ferric iron in anaerobic sediments. Applied and Environmental Microbiology 51 (4), 683–689.
Lovley, D.R., Phillips, E.J., Lonergan, D.J., 1991. Enzymic versus nonenzymic mechanisms for iron (iii) reduction in aquatic sediments. Environmental Science & Technology 25 (6), 1062–1067.
Manzoni, S., Porporato, A., 2007. A theoretical analysis of nonlinearities and feedbacks in soil carbon and nitrogen cycles. Soil Biology and Biochemistry 39 (7), 1542–1556.
Mengel, K., 1994. Iron availability in plant tissues-iron chlorosis on calcareous soils. Plant and Soil 165 (2), 275–283.
Mori, S., 1999. Iron acquisition by plants. Current Opinion in Plant Biology 2 (3), 250–253.
Pasakarnis, T., McCormick, M.L., Parkin, G.F., Thompson, A., Scherer, M.M., 2015. Feiiaq–feiiioxide electron transfer and fe exchange: effect of organic carbon. Environmental Chemistry 12 (1), 52–63.
Porporato, A., Dodorico, P., Laio, F., Rodriguez-Iturbe, I., 2003. Hydrologic controls on soil carbon and nitrogen cycles. i. modeling scheme. Advances in Water Resources 26 (1), 45–58.
Robin, A., Vansuyt, G., Hinsinger, P., Meyer, J.M., Briat, J.-F., Lemanceau, P., 2008. Iron dynamics in the rhizosphere: consequences for plant health and nutrition. Advances in Agronomy 99, 183–225.
Robinson, N.J., Procter, C.M., Connolly, E.L., Guerinot, M.L., 1999. A ferric-chelate reductase for iron uptake from soils. Nature 397 (6721), 694.
Roden, E.E., Wetzel, R.G., 1996. Organic carbon oxidation and suppression of methane production by microbial fe (iii) oxide reduction in vegetated and unvegetated freshwater wetland sediments. Limnology & Oceanography 41 (8), 1733–1748.
Rodríguez-Iturbe, I., Porporato, A., 2004. Ecohydrology of Water-Controlled Ecosystems: Soil Moisture and Plant Dynamics. Cambridge University Press.
Saaltink, M.W., Pifarré, F.B., Ayora, C., Carrera, J., Pastallé, S.O., 2004. Retraso, a code for modeling reactive transport in saturated and unsaturated porous media. Geológica Acta 2 (3), 235–251.
Scatena, F.N., 1989. An introduction to the physiography and history of the bisley experimental watersheds in the luquillo mountains of Puerto Rico. In: Gen. Tech. Rep. SO-72, vol. 22. US Dept of Agriculture, Forest Service, Southern Forest Experiment Station, New Orleans, LA, pp. 72.
Stumm, W., Morgan, J.J., 2012. Aquatic Chemistry: Chemical Equilibria and Rates in Natural Waters, vol. 126 John Wiley & Sons.
Suarez, D.L., Simunek, J., 1997. Unsatchem: unsaturated water and solute transport model with equilibrium and kinetic chemistry. Soil Science Society of America Journal 61 (6), 1633–1646.
Thompson, A., Chadwick, O.A., Rancourt, D.G., Chorover, J., 2006. Iron-oxide crystallinity increases during soil redox oscillations. Geochimica et Cosmochimica Acta 70 (7), 1710–1727.
Todd-Brown, K.E., Hopkins, F.M., Kivlin, S.N., Talbot, J.M., Allison, S.D., 2012. A framework for representing microbial decomposition in coupled climate models. Biogeochemistry 109 (1–3), 19–33.
Weber, K.A., Achenbach, L.A., Coates, J.D., 2006. Microorganisms pumping iron: anaerobic microbial iron oxidation and reduction. Nature Reviews Microbiology 4 (10), 752–764.
Weiss, J.V., Emerson, D., Megonigal, J.P., 2004. Geochemical control of microbial fe (iii) reduction potential in wetlands: comparison of the rhizosphere to non-rhizosphere soil. FEMS Microbiology Ecology 48 (1), 89–100.
Weiss, J.V., Emerson, D., Megonigal, J.P., 2005. Rhizosphere iron (iii) deposition and reduction in a l.-dominated wetland. Soil Science Society of America Journal 69 (6), 1861–1870.
Yang, W.H., Liptzin, D., 2015. High potential for iron reduction in upland soils. Ecology 96 (7).
Yeh, G.-T., Tripathi, V.S., 1991. A model for simulating transport of reactive multispecies components: model development and demonstration. Water Resources Research 27 (12), 3075–3094.
Zhao, Q., Poulson, S.R., Obrist, D., Sumaila, S., Dynes, J.J., McBeth, J.M., Yang, Y., 2016. Iron-bound organic carbon in forest soils: quantification and characterization. Biogeosciences 13 (16).
Zou, X., Zucca, C.P., Waide, R.B., McDowell, W.H., 1995. Long-term influence of deforestation on tree species composition and litter dynamics of a tropical rain forest in Puerto Rico. Forest Ecology and Management 78 (1–3), 147–157.